Available online at www.sciencedirect.com

ScienceDirect

Nuclear Physics A 967 (2017) 43–50

www.elsevier.com/locate/nuclphysa

Highlights of experimental results from ALICE

Anthony Timmins for the ALICE Collaboration

406C Science & Research, Building 1, Department of Physics, University of Houston, Houston, TX 77204, United States

Abstract

Highlights of recent results from the ALICE collaboration are presented. The collision systems investigated are Pb–Pb, p–Pb, and pp, and results from studies of bulk particle production, azimuthal correlations, open and hidden heavy flavor, and hard probes are shown. The results provide key constraints on transport properties of the QCD matter, the initial conditions, the dynamics of heavy quarks in hot and dense systems, and the coupling of hard probes with the medium. A brief description of the ALICE upgrade program is also given.

1. Introduction

ALICE is the only dedicated heavy-ion experiment at the Large Hadron Collider (LHC), and has an extensive set of sub-detectors which can probe a broad set of observables from heavy-ion and elementary collisions. The ALICE collaboration presented 28 parallel talks and over 60 posters at this Quark Matter conference. The results presented are based on data sampled from LHC running period 1, and the ongoing running period 2. Table 1 shows the corresponding collisions particle species and center of mass energies for those periods. The integrated luminosities obtained in running period 2 were significantly higher than running period 1.

Running Period 1 (2009-2013)	**Running Period 2 (2015-present)**
Pb–Pb $\sqrt{s_{\mathrm{NN}}}$ = 2.76 TeV	Pb–Pb $\sqrt{s_{\mathrm{NN}}}$ = 5.02 TeV
p–Pb $\sqrt{s_{\mathrm{NN}}}$ = 5.02 TeV	p–Pb $\sqrt{s_{\mathrm{NN}}}$ = 5.02, 8 TeV
pp $\sqrt{s}$ = 0.9, 2.76, 7, 8 TeV	pp $\sqrt{s}$ = 5, 13 TeV

Table 1. Overview of collisions systems and energies investigated at the LHC.

The primary detector of ALICE is the Time Projection Chamber (TPC), which measures charged particles via their ionization trails in the gaseous region. The TPC has an angular acceptance of $0 < \varphi < 2\pi$, $|\eta| < 0.9$ for tracks with full radial track length, and $|\eta| < 1.5$ for tracks of reduced length. Information from the Inner Tracking System (ITS) is used to improve the spatial resolution of TPC tracks, which helps with the rejection of secondary tracks and to improve the momentum resolution. Primary vertex information is

http://dx.doi.org/10.1016/j.nuclphysa.2017.07.013

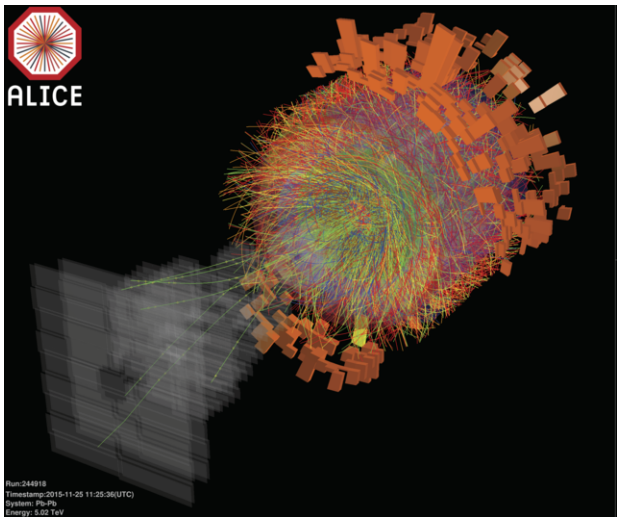

Fig. 1. Event display for a single Pb–Pb $\sqrt{s_{\rm NN}}$ = 5.02 TeV 0 – 5% central collision.

provided by the TPC and the Silicon Pixel Detector (SPD). Two VZERO counters, each containing two arrays of scintillator tiles and covering $2.8 < \eta < 5.1$ (VZERO-A) and $-3.7 < \eta < -1.7$ (VZERO-C), provide information for triggering and event class determination. The Forward Multiplicity Detector (FMD) detects charged particles in the ranges $-3.5 < \eta < -1.7$ and $1.7 < \eta < 5.0$, while the Muon Spectrometer covers the range $2.5 < \eta < 4$. The Zero Degree Calorimeters (ZDCs), located 115 meters away from the interaction point, measures spectator neutrons from heavy-ion collisions. At mid-rapidity, particle identification can be carried out using the TPC and ITS, as well as the Time of Flight (TOF) detector and the High Momentum Particle Identification Detector (HMPID). The Transition Radiation Detector (TRD) is used for electron identification. The Electro-Magnetic Calorimeter (EMCal) is primarily used to detect high momentum neutral particles at mid-rapidity. A more detailed description of the ALICE detector can be found elsewhere [1]. In Fig. 1, we show an ALICE event display from a Pb–Pb $\sqrt{s_{\rm NN}}$ = 5.02 TeV 0 – 5% collision. Using the extensive η range provided by the various subdetectors, we are able to determine that 21400 ± 1300 charged particles are produced over full phase space in such collisions [2, 3].

2. Bulk Particle Production

The light flavor particles comprise of the majority of the particles produced, and as mentioned, the ALICE detector has extensive capabilities regarding particle identification. In Fig. 2, we show inclusive π and p spectra from Pb–Pb $\sqrt{s_{\rm NN}}$ = 5.02 TeV collisions [4]. All four of our charged hadron PID detectors (TPC, ITS, TOF, HMPID) were used. The increasing radial flow with increasing centrality is particularly evident in the p spectra, where the peak shifts to progressively larger values. A Blast Wave fit was performed on the π, K, and p spectra simultaneously [5], and the obtained radial flow velocities are the highest ever observed from heavy-ion collisions ($\langle\beta_T\rangle \sim 0.66$). First measurements of event-by-event net particle moments were also presented [6]. Ratios of different order moments can be directly compared to Lattice QCD calculations, and provide information of the system such as the chemical freeze out temperature. In particular, the second order net proton moments were shown, and it was found these moments are consistent with the expectations from a Skellam distribution, with small corrections for baryon number conservation. The Skellam distribution assumes the distributions of single (anti) protons are Poissonian and independent.

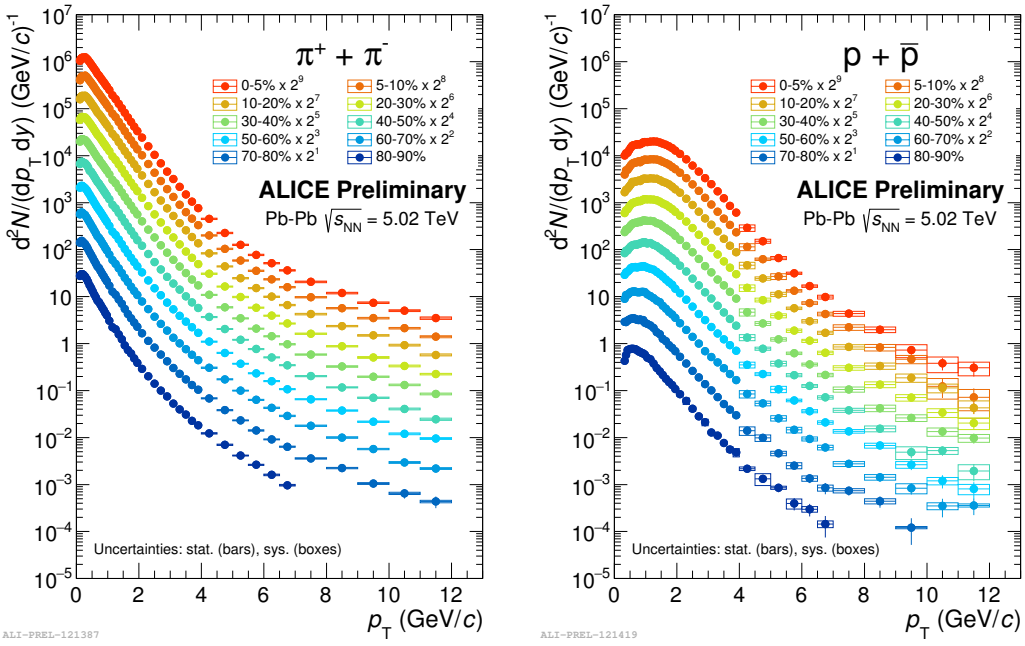

Fig. 2. Mid-rapidity inclusive π and p spectra as a function of centrality from Pb–Pb $\sqrt{s_{\mathrm{NN}}}$ = 5.02 TeV collisions [4]

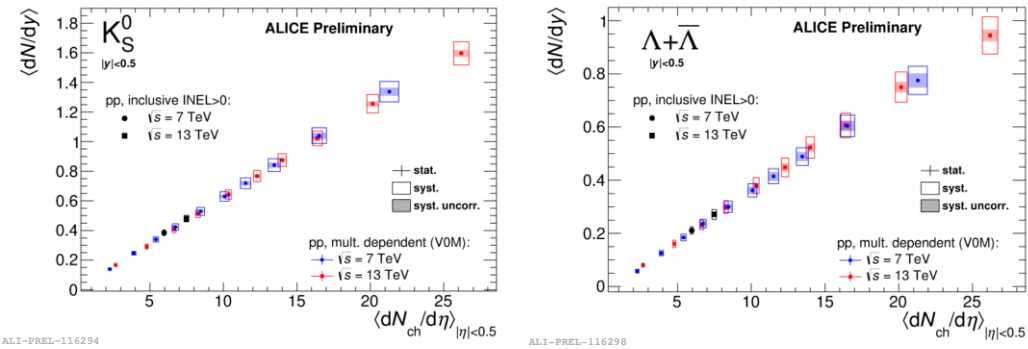

Fig. 3. Yields of strange particles as a function of charged hadron multiplicity from pp $\sqrt{s}$ = 7 and 13 TeV collisions [7].

In Fig. 3, we show yields of singly strange particles as a function of charged hadron multiplicity in pp collisions [7]. We find strangeness production scales perfectly with multiplicity when comparing the two energies, and this feature extends to the multi-strange hadrons. Measurements of π^0 and η spectra in pp $\sqrt{s}$ = 2.76 TeV collisions with unprecedented p_{T} coverage were also shown, and pQCD inspired models were found to describe the spectra over many orders of magnitude [8, 9].

3. Azimuthal Correlations

Measurements of global hyperon polarization with respect to the reaction plane are sensitive to both the vorticity and magnetic field created in heavy-ion collisions. The results from RHIC show decreasing Λ and $\bar{\Lambda}$ polarization values with energy [10], and our results are shown in the left panel of Fig. 4. They are consistent with extremely small values (less than 0.1%) at the LHC. The Chiral Magnetic Effect (CME) is also driven by the presence of a magnetic field, and the corresponding charge separation along the magnetic field direction may be indicative of parity violation in the strong interaction. The charge separation can be characterized by the γ correlator [12], which is the difference of the three-particle correlator $\langle\cos(\varphi_a + \varphi_b + 2\Psi_2)\rangle$ for opposite and same sign pairs. However, there have been recent indications that a combination of elliptic flow and charge conservation contribute to this correlator as background [13]. In order to disentangle signal and background, we have employed the Event Shape Engineering technique [14], which can be used to vary the eccentricity (therefore the elliptic flow) for a given centrality. Using initial state model calculations to determine the variation of the magnetic field, we are able to determine the fraction of the CME signal contributing to the the γ correlator. That fraction is shown in the right panel of Fig. 4. Integrating over a wide centrality range (10-50%), we find that the fraction has a 1σ upper limit of $\sim 20\%$.

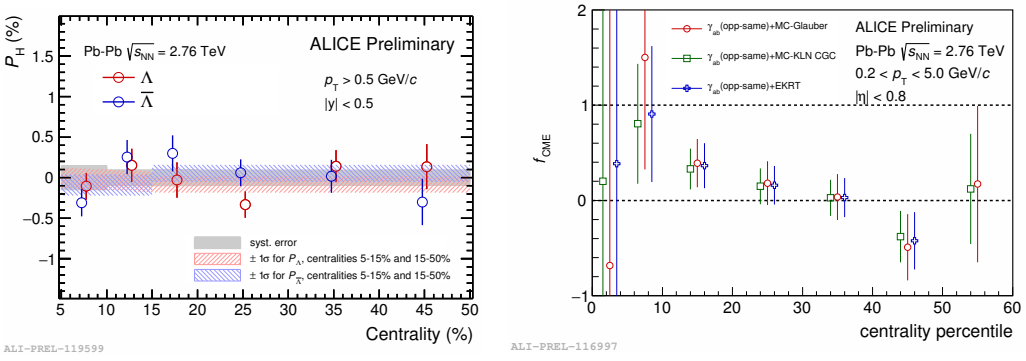

Fig. 4. Left Panel: Measurements of global hyperon polarization in Pb–Pb $\sqrt{s_{\mathrm{NN}}}$ = 2.76 TeV collisions [11]. Right Panel: Estimate of fraction of CME signal using ESE from Pb–Pb $\sqrt{s_{\mathrm{NN}}}$ = 2.76 TeV collisions [12].

In Fig. 5, we show our identified particle v_2 from Pb–Pb $\sqrt{s_{\mathrm{NN}}}$ = 5.02 TeV collisions [15]. These measurements were compared to predictions from the hydrodynamic models, and are sensitive to the hadronization mechanism and radial flow. Compared to previous ALICE results at lower energy [16], the increased precision of ϕ measurement shows a clear grouping with the protons at low p_{T} (similar mass), and the mesons at mid p_{T} (same quark number). It was found that v_2 for different species becomes similar at high p_{T} ($p_{\mathrm{T}} \gtrsim 10$ GeV/c). Given that anisotropies in this region are believed to be driven by the differences in in-plane and out-plane jet quenching, these results show such quenching is flavor independent. This hypothesis is confirmed by the similar behaviour of the light hadron R_{AA}, which also converges at high p_{T} for different particle species [7]. Studies which attempt to decompose higher order azimuthal flow vectors in terms of contributions from lower order vectors were also shown [17]. The extracted measurement is χ_{mn}, and when

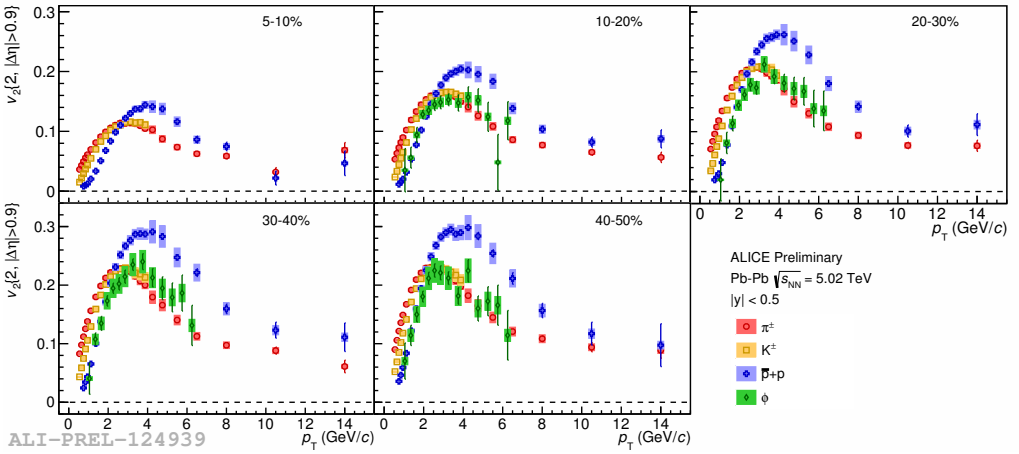

Fig. 5. Identified particle v_2 from Pb–Pb $\sqrt{s_{\rm NN}}$ = 5.02 TeV collisions [15].

this is zero, higher order flow harmonics are proportional to the corresponding eccentricity. For example, expressing the flow vector as $V_n = v_n e^{in\Psi_n}$, the 4th order vector can be decomposed as;

$$V_4 = \chi_{442}(V_2)^2 + V_4^L \tag{1}$$

We find non-zero values of χ_{mn}, and they indicate significant contributions from lower orders. The non-linear coefficients χ_{mn} were found to have different sensitivities to the initial anisotropy and the viscosity of the medium, and can be used to disentangle the two effects.

4. Open and Hidden Heavy Flavor

The transport parameters that govern heavy quark interactions with the medium in heavy-ion collisions can be calculated by various approaches e.g. perturbative QCD, effective potential models from lattice QCD, and AdS/CFT. The generation of heavy quark v_2 is sensitive to these transport parameters, and we show measurements of J/Ψ v_2 (event plane method) from Pb–Pb $\sqrt{s_{\rm NN}}$ = 5.02 TeV collisions in Fig. 6. These are the first measurements that show definitively that the charm quark flows at the LHC. Comparisons to the open heavy-flavor D mesons are also shown for the same energy. There are differences at low $p_{\rm T}$, presumably related to the differences in light and heavy quark flow. Such comparisons should help constrain the hadronization mechanisms of the charm quark.

In the left panel of Fig. 7, we show D meson nuclear modification factor $R_{\rm AA}$ as a function of $p_{\rm T}$ from Pb–Pb $\sqrt{s_{\rm NN}}$ = 5.02 TeV collisions [18]. A suppression is observed over the whole $p_{\rm T}$ range, which is qualitatively reproduced by the various model calculations. However, there is clearly an ambiguity regarding the model calculations, which can be potentially resolved by comparing other measurements (e.g. v_2) with the same models. Heavy Flavor Decay Muon $R_{\rm AA}$ as a function of $p_{\rm T}$ were shown [20], and we found little (if any) energy dependence when comparing Pb–Pb collisions with $\sqrt{s_{\rm NN}}$ = 2.76 and 5.02 TeV up to $p_{\rm T} \sim 20$ GeV/c. Moving back to hidden heavy-flavor, measurements of integrated J/Ψ $R_{\rm AA}$ were shown for both the J/$\Psi \rightarrow e^+ + e^-$ and J/$\Psi \rightarrow \mu^+ + \mu^-$ channels from Pb–Pb $\sqrt{s_{\rm NN}}$ = 5.02 TeV collisions [19, 21]. Transport models including both in-medium dissociation and recombination effects were able to reproduce the observed suppressions reasonably well.

In the right panel of Fig. 7 we show J/Ψ $R_{\rm AA}$ as a function of rapidity (y_{cms}) from p–Pb $\sqrt{s_{\rm NN}}$ = 8 TeV collisions [19], which help constrain the initial state and cold nuclear matter effects relevant for the

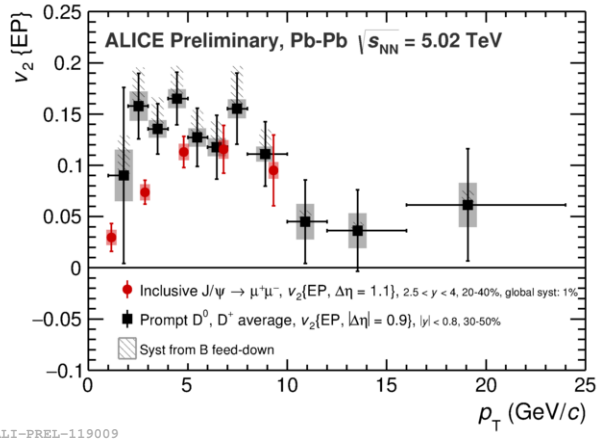

Fig. 6. Open and hidden heavy flavor v_2 from Pb–Pb $\sqrt{s_{\rm NN}}$ = 5.02 TeV collisions [18, 19]

heavy-ion measurements. A suppression is observed in the p going direction, while R_{AA} is consistent with 1 in the Pb going direction. The various models (shadowing, energy loss, CGC) appear to describe the $y_{\rm cms}$ dependence. For the p going direction, R_{AA} as a function of $p_{\rm T}$ was found to be most suppressed at low $p_{\rm T}$ and consistent with 1 at $p_{\rm T} > 6$ GeV/c. The same models explored in the right panel of Fig. 7 were found to describe the $p_{\rm T}$ dependence. Regarding J/Ψ production in pp $\sqrt{s}$ = 13 TeV collisions, the yields were shown to scale approximately linearly with the charge hadron multiplicity [22]. This dependence was described rather well with phenomenological models including Multiple Parton Interactions. Our first di-electron continuum results from pp $\sqrt{s}$ = 13 TeV collisions where also shown, and we found no change in shape comparing low to high multiplicity collisions [23].

5. Hard Probes

The jet mass is sensitive to the initial virtuality of the parton at the origin of the shower, and may temporarily increase in a hot QCD medium, leading to a larger gluon radiation probability [25]. It is defined as the difference between the energy of the jet ($E_{\rm jet}$) and its transverse ($p_{\rm T,jet}$) and longitudinal ($p_{\rm z,jet}$) momentum:

$$M_{\rm jet} = \sqrt{E^2_{\rm jet} - p^2_{\rm T,jet} - p_{\rm z,jet^2}} \tag{2}$$

Our first measurements of the average jet mass for reconstructed charged hadron jets in Pb–Pb $\sqrt{s_{\rm NN}}$ = 2.76 TeV collisions are shown in the left panel of Fig. 8, where the average mass increases with jet $p_{\rm T}$ [24]. Models with quenching (JEWEL+PYTHIA recoil on and Q-PYTHIA) indeed predict larger values compare to the vacuum model (PYTHIA Perugia 2011 tunes), however, somewhat surprisingly, the vacuum model is closer to the data. The p–Pb $\sqrt{s_{\rm NN}}$ = 5.02 TeV measurements were also consistent with Pb-Pb, perhaps indicating that much of the extra gluon radiation is outside of the jet cone. Our first measurements of N-subjettiness (τ_2/τ_1) in Pb–Pb $\sqrt{s_{\rm NN}}$ = 2.76 TeV collisions were also presented [27]. The ratio of τ_2/τ_1 extracted from jets and is inversely related to the probability of the leading parton splitting into two resolvable partons. The presence of a hot medium shifts τ_2/τ_1 to higher values. However, as with our jet mass measurements, the data from heavy-ion collisions were consistent with vacuum expectations from the PYTHIA model. The effects of jet quenching were more readily seen in the associated yield ratio of $I_{\rm AA}$ from two-particle correlations using π^0 particles as the trigger [8, 26]. For the associated charged hadron yields at low $p_{\rm T}$, an enhancement was seen on the near-side, which was even greater with respect to the

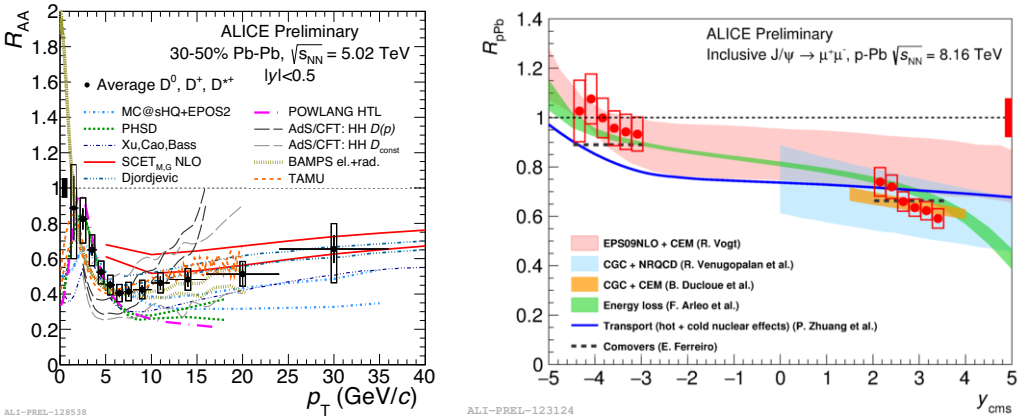

Fig. 7. Left panel: Open heavy-flavor R_{AA} as a function of transverse momentum [18]. Right Panel: Integrated R_{pPb} for J/ψ as a function of rapidity [19].

away-side. At higher p_T, the near-side I_{AA} approaches one, while the away-side I_{AA} becomes smaller than one.

In order to investigate possible jet quenching in light systems, measurements of the recoil jet yield were carried out, which extract the number of away-side reconstructed jets per hadron trigger [28]. While the away-side jet yields are suppressed in central Pb–Pb $\sqrt{s_{\mathrm{NN}}}$ = 2.76 TeV collisions relative to peripheral, the right panel of Fig. 8 shows no such suppression in high multiplicity p–Pb $\sqrt{s_{\mathrm{NN}}}$ = 5.02 TeV collisions. We also presented near-side peak widths of two-particle correlations from pp $\sqrt{s}$ = 13 TeV collisions as a function of multiplicity [29]. Unlike the case Pb–Pb $\sqrt{s_{\mathrm{NN}}}$ = 2.76 TeV collisions [30], the widths were found to be constant, and well reproduced by the PYTHIA model.

6. Upgrades

ALICE is undergoing an extensive upgrade program, and there were two parallel presentations reviewing two of the projects within that program. The first presentation detailed the TPC upgrade [31], which will be the first application of GEM technology in a large scale TPC readout. In continuous readout mode, the TPC will be able to record events at rates 50 times larger than its current ability. The second presentation discussed the ITS upgrade [32]. This will involve the largest application of Si pixel sensors in a single detector, with improved data recording rates and hit precision. Both upgrades will be complete by running period 3, which is expected to start in the early 2020s.

7. Summary

Using the high precision data from running period 2, we have observed the largest ever radial flow velocities from heavy-ion collisions. At higher p_T, we observed that light flavor v_2 for different species becomes similar at high p_{T} ($p_{\mathrm{T}} \gtrsim 10$ GeV/c). A similar pattern is seen for R_{AA}, and indicates flavor independent quenching controls these observables. We have shown the first direct evidence of charm quark elliptic flow at the LHC, and coupled with our R_{AA} measurements, these place stronger constraints on heavy quark medium interactions. Using data from running period 1, we have shown the first net particle moments at the LHC. We have also placed strong constraints on background contributions to the CME signal, and shown a new set of jet observables which can probe aspects of interactions between fast partons in the hot and dense medium.

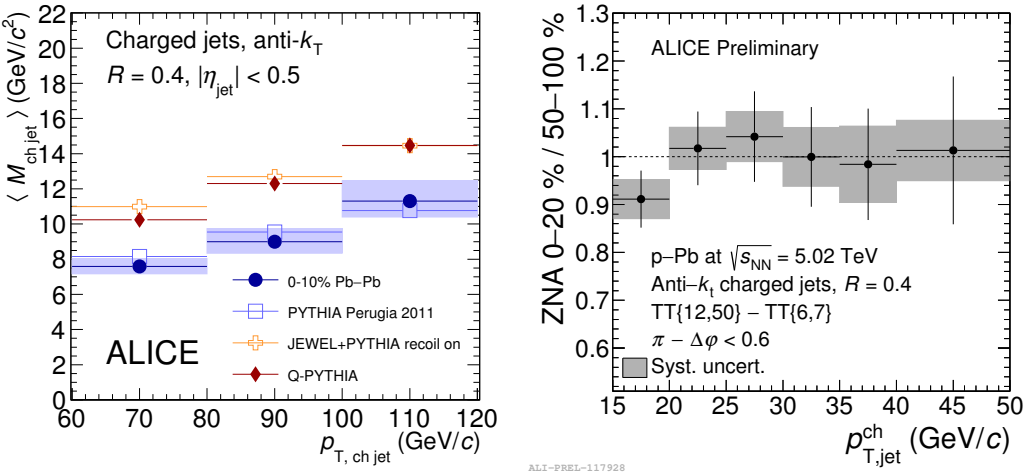

Fig. 8. Left panel: Average charged jet mass as a function of the jet transverse momentum in Pb–Pb $\sqrt{s_{NN}}$ = 2.76 TeV collisions [24, 25]. Right Panel: Relative number of away-side jets in high multiplicity compared to low multiplicity p–Pb $\sqrt{s_{NN}}$ = 5.02 TeV collisions as a function of the jet transverse momentum [28].

References

[1] K. Aamodt *et al.* (ALICE Collaboration), JINST **3** (2008) S08002.
[2] C. H. Christensen (ALICE Collaboration), *these proceedings*
[3] J. Adam (ALICE Collaboration), *arXiv:1612.08966*
[4] N. Jacazio (ALICE Collaboration), *these proceedings*
[5] F. Retiere and M. Lisa, Phys. Rev. C **70** (2004) 044907
[6] A. Rustamov (ALICE Collaboration), *these proceedings*
[7] V. Vislavicius (ALICE Collaboration), *these proceedings*
[8] A. Vauthier (ALICE Collaboration), *these proceedings*
[9] S. Acharya et al. (ALICE Collaboration), *arXiv:1702.00917*
[10] I. Upsal (STAR Collaboration), *these proceedings*
[11] M. Konyushikhin (ALICE Collaboration), *poster presented*
[12] A. Dobrin (ALICE Collaboration), *these proceedings*
[13] V. Khachatryan et al. (CMS Collaboration), Phys. Rev. Lett. **118** (2017) 122301
[14] J. Schukraft, A. Timmins and S. Voloshin, Phys. Lett. B **719** (2013) 394-398
[15] R. Bertens (ALICE Collaboration), *these proceedings*
[16] B. Abelev et al. (ALICE Collaboration), JHEP **06** (2015) 190
[17] Y. Zhou (ALICE Collaboration), *these proceedings*
[18] A. Barbano (ALICE Collaboration), *these proceedings*
[19] M. Tarhini (ALICE Collaboration), *these proceedings*
[20] D. Moreira de Godoy (ALICE Collaboration), *these proceedings*
[21] T. Jimenez (ALICE Collaboration),*these proceedings*
[22] S. Weber (ALICE Collaboration), *these proceedings*
[23] O. Vazquez Doce (ALICE Collaboration), *these proceedings*
[24] D. Caffarri (ALICE Collaboration), *these proceedings*
[25] S. Acharya et al. (ALICE Collaboration), *arXiv:1702.00804*
[26] S. Acharya et al. (ALICE Collaboration), Phys. Lett. B **763** (2016) 238-250
[27] N. Zardoshti (ALICE Collaboration), *these proceedings*
[28] F. Krizek (ALICE Collaboration), *these proceedings*
[29] I. Lakomov (ALICE Collaboration),*these proceedings*
[30] J. Adam (ALICE Collaboration), *arXiv:1609.06643 and arXiv:1609.06667*
[31] R. Majka (ALICE Collaboration), *these proceedings*
[32] P. Martinengo (ALICE Collaboration), *these proceedings*